Active Sensor Wave Propagation Health Monitoring of Beam and Plate Structures

Victor Giurgiutiu, Jingjing Bao, Wei Zhao
University of South Carolina

ABSTRACT

Active sensor wave propagation technique is a relatively new method for in-situ nondestructive evaluation (NDE). Elastic waves propagating in material carry the information of defects. These information can be extracted by analyzing the signals picked up by active sensors. Due to the physical property of wave propagation, large area can be interrogated by a few transducers. This simplifies the process of detecting and characterizing defects. To apply this method, efficient numerical modeling is required to predict signal amplitude and time history of elastic wave scattering and diffraction. In order to construct the model, good understanding of these physical phenomena must be achieved.

This paper presents results of an investigation of the applicability of active sensors for in-situ health monitoring of aging aircraft structures. The project set forth to develop non-intrusive active sensors that can be applied on existing aging aerospace structures for monitoring the onset and progress of structural damage such as fatigue cracks and corrosion. Wave propagation approach was used for large area detection. In order to get the theoretical solution of elastic wave propagating in the material, wave functions of axial wave, share wave, flexure wave, Raleigh wave, and Lamb waves were thoroughly investigated. The wave velocities and the motion of these different types of waves were calculated and simulated using mathematical analysis programs. Finite Element Method was used to simulate and predict the wave propagating through the structure for different excitation and boundary conditions. Aluminum beams and plates were used to get experiment results. Structures both pristine and with known defects are used in our investigation. The experimental results were then compared with the theoretical results.

Keywords: in-situ diagnostics, health monitoring, piezoelectric, ultrasonic, Lamb wave, dispersion

1.   INTRODUCTION

Piezoelectric excitation of isotropic and anisotropic structures was initially studied for structural control. Crawley and Lazarus (1991) developed piezoelectric sensor and actuator relations using equivalent line moments. This work was extended by Jia and Rogers (1989), Tzou and Tseng (1990), Dimitriadis *et al.* (1991), Lester and Lefebvre (1993), Song and Librescu (1998), and others. Royston (1998) performed modeling, analysis, and experimental investigation smart-materials nonlinear dynamics for structural vibro-acoustic control. Saravanos and Heyliger (1994) developed a unified approach for laminated beams with incorporated piezo-electric elements. Hall and Flatau (1998) studied the analog feedback control for magnetostrictive transducer linearization. Damage detection through built-in piezoelectrics was pioneered by Keilers and Chang (1995) for delamination identification in composite plates. Various damage detection criteria, e.g., based on wave propagation, are also being studied (Chang, 1998). Lakshmanan and Pines (1997) used wave propagation to detect transverse cracks in a rotating composite beam from the structural scattering properties. Saravanos, Birman, and Hopkins (1996) modeled the delamination detection in a composite beam using surface mounted piezoelectric sensors. Moetakef, Joshi, and Lawrence (1996) performed finite-element modeling and experimental study of elastic waves generation through equally spaced piezoceramic wafers. Blanas *et al.* (1997, 1998) studied the use of active composites sensors for acoustic-emission health monitoring. Liang *et al.* (1996) developed an impedance method for dynamic analysis of active material systems. Giurgiutiu and Rogers (1998a,b) used the electro-mechanical (E/M) impedance technique for structural health monitoring and performed multiple damage-detection experiments. Pardo de Vera and Guemes (1997) used embedded self-sensing piezoelectrics for damage detection of small composite specimens. Quattrone *et al.* (1998) use the same method to detected the onset of delamination in a composite-on-masonry 4-ft by 4-ft specimen under static testing, Quinn *et al.* (1999) are developing new damage identification, localization, and quantification techniques. Osmont *et al* (2000) are using Lamb waves propagation in sandwich plates to identify the effect of impact damage in sandwich skins and core. Diaz-Valdes and Soutis (2000) have experimentally and theoretically studied the propagation of low-frequency Lamb waves in fiber composite laminates for real-time non-destructive evaluation.

This paper presents results of an investigation of the applicability of active sensors for in-situ health monitoring of aging aircraft structures. The project set forth to develop non-intrusive active sensors that can be applied on existing aging aerospace structures for monitoring the onset and progress of structural damage such as fatigue cracks and corrosion.

2. REVIEW OF WAVE PROPAGATION THEORY

In order to use ultrasonic waves in NDE, different types of waves must be studied to understand the undergoing physical phenomena. The objective is to model the wave propagation for different type of ultrasonic sound waves, and use the available software to visualize these waves. Wave is a disturbance that travels, or propagates, from one region of space to another. Table 1 below shows some of the wave modes possible in solids.

Table 1 Waves in solids

wave type	particle vibrations
Longitudinal / Compressional / Dilatational Wave	parallel to the direction of propagation
Tansverse / Shear / Distortional Wave	Perpendicular to the direction of the propagation of the wave
Surface (Rayleigh)	Elliptical orbit - symmetrical mode
Plate Wave - Lamb	Component perpendicular to surface

To achieve further understanding of waves, visualization of the waveforms was done. Putting the wave equations into mathematics software, the particles' displacement as function of space and time was calculated. The resultant displacement can be shown in an array of vectors, which is like a "snapshot" of the particles at that moment. By showing the "snapshots" in the order of time, the propagation of the wave can be animated. The wave figures in the following sections are part of the result of this effort. Animations of waves were posted on the Internet at: http://www.engr.sc.edu/research/lamss/default.htm under the research section.

2.1 Longitudinal wave

Longitudinal wave is also called compressional wave, axial wave dilatational wave, pressure wave, or P-wave. For this type of wave motion, the particle displacement is parallel to the direction of propagation. The wave function can be written as:

$$y(x,t) = A \sin \omega(t - \frac{x}{v}) = A \sin 2\pi f (t - \frac{x}{v}) = A \sin 2\pi (\frac{t}{T} - \frac{x}{\lambda}) \tag{1}$$

If we define wave number, $k = \frac{2\pi}{\lambda}$, then, $y(x,t) = A \sin(\omega t - kx)$, where $c_P = \sqrt{E/\rho}$, is the longitudinal wave speed in

solids, with E being the Young's modulus, and ρ the density of the solid. Equation (1) was plotted in Figure 1
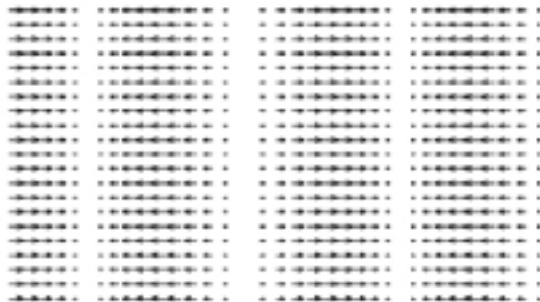

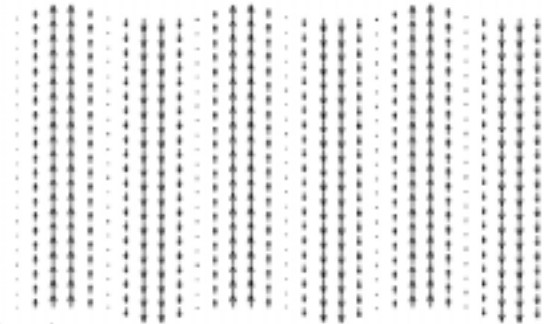Figure 1 simulation of P-wave.

Figure 2 simulation of S-wave.

2.2 Shear wave

Shear wave is also called transverse wave, shear wave, distortional wave, or S-wave. For this type of wave motion, the particle displacement is perpendicular to the direction of propagation. The wave function can be written as:

$$z(x,t) = A \sin(\omega t - kx) \tag{2}$$

If we define the Lamé constants $\lambda = \frac{v}{(1-2v)(1+v)} E$ and $\mu = \frac{E}{2(1+v)}$, then the phase velocity of the shear wave is

$c_S = \sqrt{\mu/\rho}$. Note that the longitudinal wave velocity can also be written as $c_P = \sqrt{(\lambda + 2\mu)/\rho}$. Equation (2) was plotted in Figure 2

2.3 Flexure wave

These are transverse motions resulting from bending action. The simplest theory for flexural is based on the Bernoulli-Euler theory of beams. The governing equation is:

$$\frac{\partial^4 w}{\partial x^4} + \frac{1}{a^2}\frac{\partial^2 w}{\partial t^2} = 0 .$$ (3)

Where $a^2 = \dfrac{EI}{\rho A}$. The particle notion is shown in Figure 3. Assuming $w = Ae^{i(k_F x - \omega t)}$, then wave number k_F can be obtained

by solving the characteristic equation, $k_F - \dfrac{\omega^2}{a^2} = 0$, i.e. $k_F = \pm\sqrt{\dfrac{\omega}{a}}$. Since $k_F = \dfrac{\omega}{c_F}$, the flexural wave velocity

$$c_F = ak_F = \sqrt{a\omega}$$ (4)

This is a function of wave frequency ω, which means that the flexural wave velocity depends on its frequency (i.e. it is dispersive) .
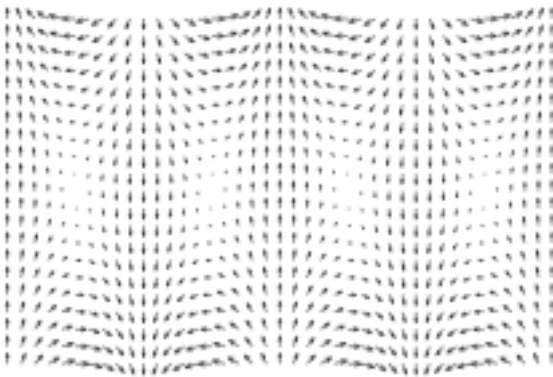

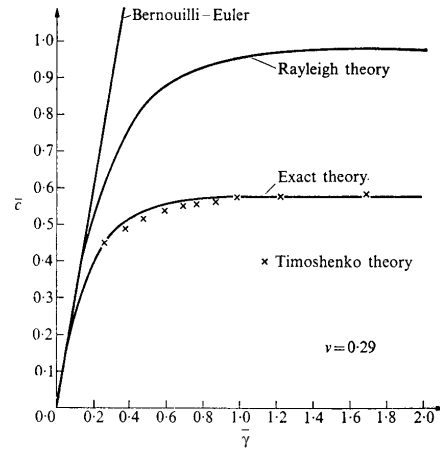Figure 3 simulation of flexure wave.

Figure 4 Dispersion relations from Timoshenko, exact, Rayleigh, and Bernoulli-Euler beam theories (Graff, 1975).

Flexural waves can also be described by more advanced theories, such as Rayleigh theory including rotary-inertia effects, Timoshenko beam theory, including rotary-inertia and shear deformation effects, or exact theory of elasticity. Comparison of

the resultant wave velocity values for different theories as function of the non-dimensional wave number, $\bar{\gamma} = \dfrac{ak_F}{2\pi}$, is given

in Figure 4. It should be noted that the exact theory predicted a leveling off of the flexural speed at high frequency.

2.4 Rayleigh wave

These surface waves were named after Lord Rayleigh, mathematical physicist, 1842-1919. In this particular type of wave which propagates on the surface of a body, motion decreases rapidly with depth below the surface. The polarization of Rayleigh waves lies in a plane perpendicular to the surface. The effective depth of penetration is less than a wavelength. Unwanted waves may be generated at the entry surface by shear wave probes of 70° angle or over. They are also responsible for cross noise.
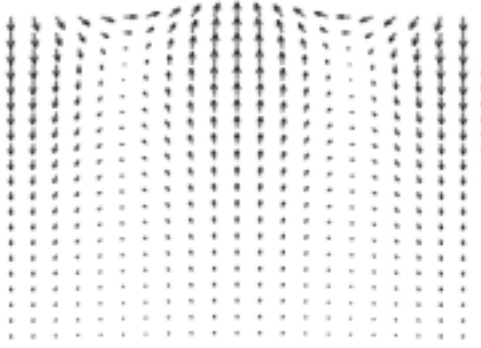
Figure 5 Simulation of Rayleigh wave.

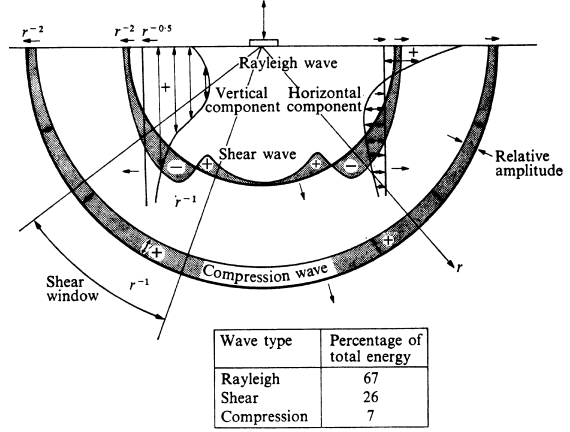| Wave type	Percentage of total energy
Rayleigh	67
Shear	26
Compression	7

Figure 6 Distribution of displacement and energy in dilatational, shear, and Rayleigh waves generated in elastic half-space by a harmonic normal load (after Woods, 1968).

The Rayleigh wave can be decomposed into the horizontal component, U, and the vertical component, W. Both U and W are functions of x, z, and t, where x and z are the dimension of the particle in media, t is time. The wave velocity of Rayleigh wave is $c_R = c_S \left(\dfrac{0.87 + 1.12\nu}{1+\nu} \right)$, and the Rayleigh wave number is $k_R = \dfrac{\omega}{c_R}$. If we define $q = \sqrt{k_R^2 - k_P^2}$ and $s = \sqrt{k_R^2 - k_S^2}$, then the two components of the particle movement can be expressed as

$$U(x,z,t) = Ak_R \left(e^{-qz} - \frac{2qs}{k_R^2 + s^2} e^{-sz} \right) \sin(k_R x - \omega t) \tag{5}$$

$$W(x,z,t) = Aq \left(e^{-qz} - \frac{2k_R^2}{k_R^2 + s^2} e^{-sz} \right) \cos(k_R x - \omega t) \tag{6}$$

Figure 5 shows the simulation of particle motion for a Rayleigh wave.

2.5 Lamb wave

These are a type of ultrasonic waves that is guided between the two parallel surfaces of the test object. For an object sufficiently thin to allow penetration to the opposite surface, e.g. a plate having a thickness of the order of a wavelength or so, Rayleigh waves degenerate into Lamb waves. Lamb waves can propagate in a number of modes, either symmetrical or antisymmetrical. The velocity depends on the product of frequency and material thickness. Lamb waves are named after Horace Lamb, in honor of his fundamental contributions to this subject. Investigations on Lamb and leaky Lamb waves have been carried out continuously since their discovery and researchers have done theoretical and experimental work for different purposes, ranging from seismology, to ship construction industry, to acoustic microscopy, and to non-destructive testing and acoustic sensors. Synonymous terms are guided wave and plate wave. To define the wave function of Lamb wave, the Rayleigh-Lamb equation must be solved to find the wave speed of Lamb wave. Define $\xi = \sqrt{c_S^2 / c_P^2}$, $\zeta = \sqrt{c_S^2 / c_L^2}$, and $\bar{d} = k_S d$; where c_L is the Lamb wave speed, and d is the half thickness of the plate. Then the Rayleigh-Lamb frequency equation can be established,

$$\frac{\tan(\sqrt{1-\zeta^2}\,\bar{d})}{\tan\sqrt{\xi^2 - \zeta^2}} + \frac{4\zeta^2 \sqrt{1-\zeta^2}\sqrt{\xi^2 - \zeta^2}}{(2\zeta^2 - 1)^2} = 0 \tag{7}$$

Lamb wave speed can be obtained by solving equation (7). Define the Lamb wave number $k_L = \dfrac{\omega}{c_L}$, and $q = \sqrt{k_L^2 - k_P^2}$, $s = \sqrt{k_L^2 - k_S^2}$, then the two components of the particle movement can be expressed as

$$U(x,z,t) = \text{Re}[Ak_L\left(\frac{\cosh(qz)}{\sinh(qd)} - \frac{2qs}{k_L^2 + s^2}\frac{\cosh(sz)}{\sinh(sd)}\right)e^{i(k_L x - \omega t \frac{\pi}{2})}] \quad (8)$$

$$W(x,z,t) = \text{Re}[Aq\left(\frac{\sinh(qz)}{\sinh(qd)} - \frac{2k_L^2}{k_L^2 + s^2}\frac{\sinh(sz)}{\sinh(sd)}\right)e^{i(k_L x - \omega t)}] \quad (9)$$

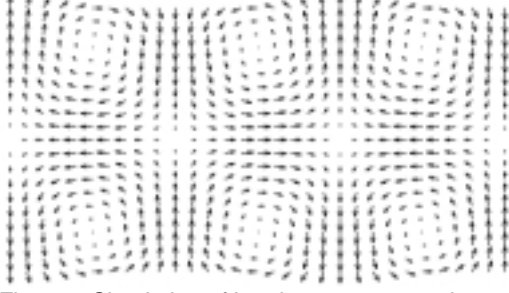Equation (8) and (9) are for the symmetric Lamb waves (Figure 7).

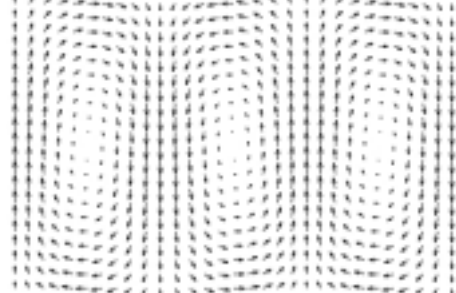Figure 7 Simulation of Lamb wave symmetric mode.

Figure 8 Simulation of Lamb wave asymmetric mode.

For asymmetric Lamb waves (Figure 8), the Rayleigh-Lamb frequency equation is

$$\frac{\tan(\sqrt{1-\zeta^2}\,\overline{d})}{\tan\sqrt{\xi^2 - \zeta^2}} + \frac{(2\zeta^2 - 1)^2}{4\zeta^2\sqrt{1-\zeta^2}\sqrt{\xi^2 - \zeta^2}} = 0. \quad (10)$$

The two component of the particle movement can be expressed as

$$U(x,z,t) = \text{Re}[Ak_L\left(\frac{\cosh(qz)}{\cosh(qd)} - \frac{2qs}{k_L^2 + s^2}\frac{\cosh(sz)}{\cosh(sd)}\right)e^{i(k_L x - \omega t \frac{\pi}{2})}] \quad (11)$$

$$W(x,z,t) = \text{Re}[Aq\left(\frac{\sinh(qz)}{\cosh(qd)} - \frac{2k_L^2}{k_L^2 + s^2}\frac{\sinh(sz)}{\cosh(sd)}\right)e^{i(k_L x - \omega t)}] \quad (12)$$

By solving the Rayleigh-Lamb frequency equation the Lamb wave speed can obtained. We computed this for two aluminum thin plate cases; (a) 2d = 1mm; and (b) 2d = 1.6mm, as shown in Figure 9. A comparison of flexural wave and 0-mode symmetric and asymmetric Lamb wave is also given in this figure. The figure shows that at low frequency flexural wave and A0 mode Lamb wave velocity are very close, but they separate at frequency higher than 200 kHz. So that the frequency will be used in health monitoring should be in high frequency (>200 kHz) to avoid interference of the two types of waves.
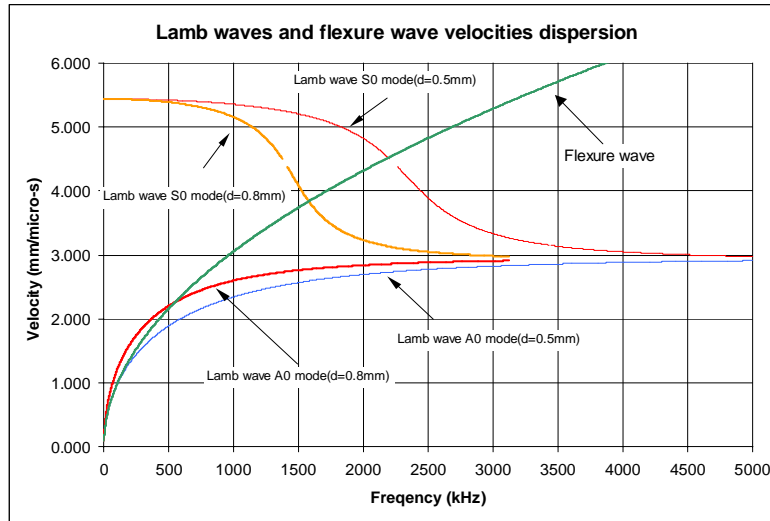

Figure 9   Wave speed dispersion curves for classical and Lamb waves in aluminum alloy medium.

3. EMBEDDED PIEZOELECTRIC ACTIVE SENSOR DEVELOPMENT FOR ULTRASONIC NDE

3.1 Modeling of the Piezoelectric Active Sensor,

The general constitutive equations of linear piezo-electric material behavior, given by ANSI/IEEE Standard 176-1987, describe a tensorial relation between mechanical and electrical variables (mechanical strain S_{ij}, mechanical stress T_{ij}, electrical field E_i, and electrical displacement D_i) in the form:

$$S_{ij} = s^E_{ijkl}T_{kl} + d_{kij}E_k$$
$$D_j = d_{jkl}T_{kl} + \varepsilon^T_{jk}E_k \,, \tag{13}$$

where s^E_{ijkl} is the mechanical compliance of the material measured at zero electric field ($E = 0$), ε^T_{jk} is the dielectric permittivity measured at zero mechanical stress ($T = 0$), and d_{kij} is the piezo-electric coupling between the electrical and mechanical variables. The second equation reflects the *direct piezo-electric effect*, while the first equation refers to the *converse piezo-electric effect*.

The piezo-electric transducers used in the ultrasonic wave propagation technique are thin Lead Zirconate Titanate (PZT) ceramic wafers intimately bonded to the surface of the host structure (Figure 10 a). In this configuration, mechanical stress and strain are applied in the 1 and 2 directions, i.e. in the plane of the surface, while the electric field acts in the 3 direction, i.e., normal to the surface. Hence, the significant electro-mechanical couplings for this type of analysis are the 31 and 32 effects. The application of an electric field, E_3, induces surface strains, S_{11} and S_{22}, and vice-versa.
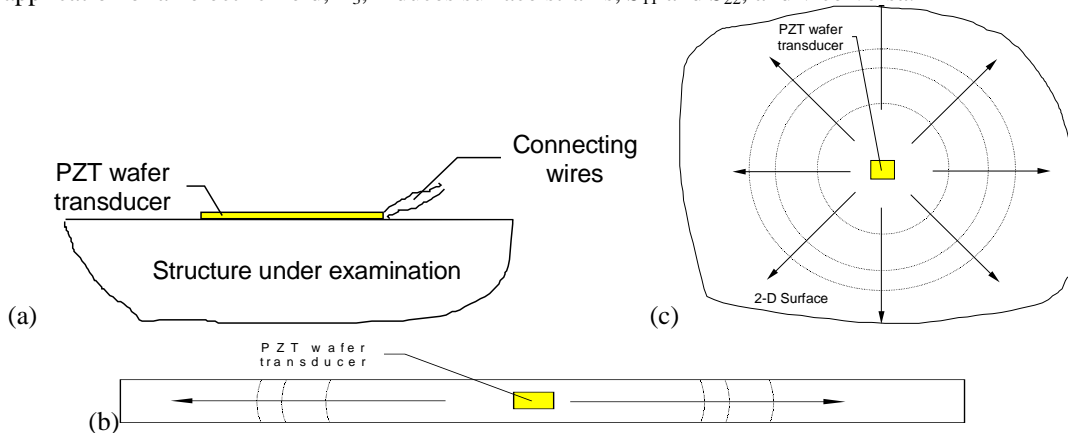

Figure 10 Piezoelectric active sensor interact with host structure: (a) PZT wafer transducer affixed to the host structure; (b) PZT wafer transducer acting on a 1-D structure; (c) PZT wafer transducer acting on a 2-D surface (Giurgiutiu, 1999)

For a PZT transducer affixed to 1-D member, e.g., a beam along the 1-direction (Figure 26 b), the analysis is mainly one-dimensional. In this case, the dominant electro-mechanical coupling constant is d_{31}. If the transducer is placed on a 2-D surface, the analysis is, in principle, two-dimensional (Figure 10c). Since the electro-mechanical coupling constants, d_{31} and d_{32}, have essentially same value, radial symmetry can be applied, and the analysis can be reduced to a one-dimensional case in the radial coordinate, r (Giurgiutiu, 1999).

3.2 Experiments on simple specimens and on realistic aging aircraft panels with simulated damage.

3.2.1 1-D specimens specification

Tests were conducted on aluminum beam to get more information of PZT wafer active sensors, and how they interact with wave propagation. The specimens intended for the experiment are presented in Figures 11. Specimen was made from aircraft grade sheet aluminum 2024 alloy, 1.6 mm thick. Piezoelectric active sensors (7 mm square, 0.2 mm thick) are installed on both sides. (The installation on both sides has been chosen to permit symmetric and anti-symmetric excitation. Thus, axial and flexural waves can be selectively excited.) The coordinates of sensor installation are given in Tables 2. The active sensors were excited with short burst of constant frequency signal (tone-burst) . Just a few sine waves (3 to 5) were used.
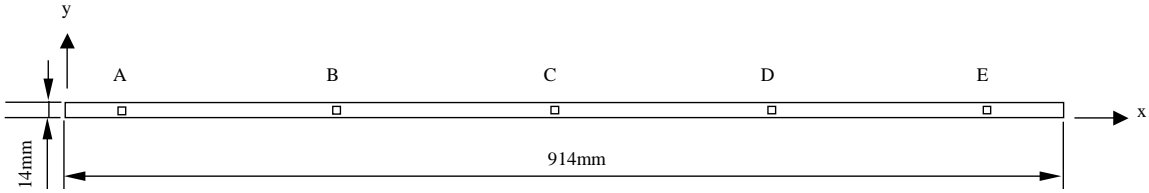
Figure 11 Beam, 1.6 mm thick, 2024 Aluminum alloy

Table 2 Locations of sensors on beam

Sensor#	A	B	C	D	E
X (mm)	57	257	457	657	857
Y (mm)	7	7	7	7	7

In the beginning level, investigations were concentrated on the simple 1-D experiments and modeling. The specimen was long beam. On this specimen, we conducted and simulated 1-D wave propagation experiments. One of the five pairs of PZT wafer transducers was used for transmission each time in a round-robin fashion, and other locations for reception.

3.2.2   Finite element analysis

Numerical simulations of the wave propagation process were performed using the commercial finite element code, ANSYS. The same beam specimen as used in the experimental measurement was modeled using 4-node shell elements (SHELL63). The element has six degrees of freedom at each node with both bending and membrane capabilities. Two forms of the elastic wave propagation are studied: the flexure wave and the pressure wave. Excitation "equivalent to" the PZT excitation were applied. In the case of the flexure wave, transient nodal rotations were applied on the nodes that represent the transverse edges of the PZT sensor. While in the case of the pressure wave, nodal translations were applied. The excitation was applied in terms of five counts of sine waves. To reduce the wave dispersion effect and facilitate the understanding of the resulting wave propagation, the excitation wass applied after

Figure 12 An example of the applied transient load

passing through a Hanning window. Fig. 12 shows the resulting form of the excitation signal. Some typical results from the simulations are shown in Figures 13 and 14.
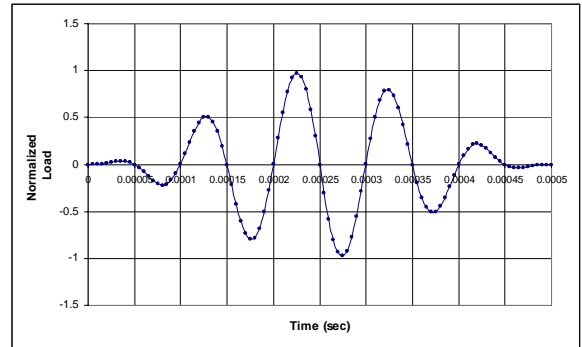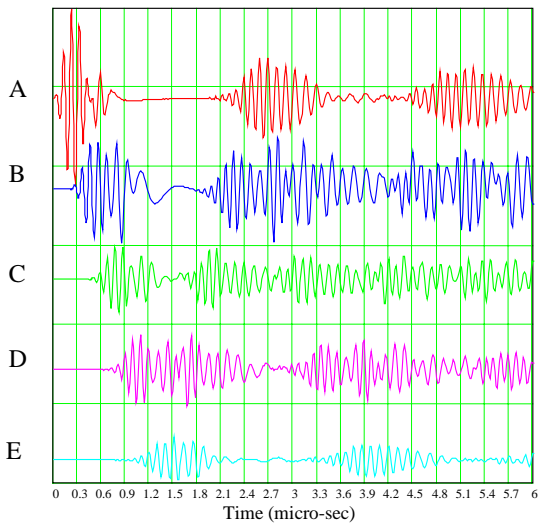

Figure 13 Result for the flexure wave, 10 kHz
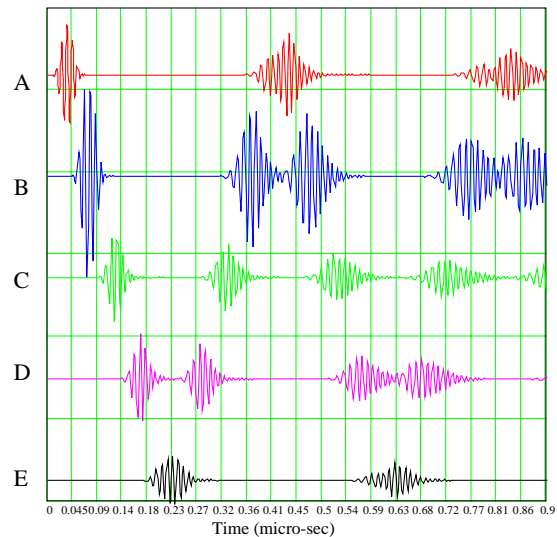

Figure 14 Result for the pressure wave, 100 kHz

7

3.2.3   Experimental results

A HP 33120A signal generator was used to generate the burst signal; a Tektronix TDS 210 digital oscilloscope and a laptop computer connected through GPIB interface were used to collect data. Burst signal was applied to PZT transducers, single and in pair. At low frequency (<100kHz), PZT transducer pairs were excited with burst signals in-phase and out-phase to test the capability of using a pair of PZT wafer transducer to enhance or surpress a certain type of wave, and to examine the wave speed of different type of waves. Due to the restriction of instrument's capability, only in-phase signal were applied at higher frequency. Figure 15 presents some data from these experiments. On each plot, signal A was the input burst signal, and B through E was the output of PZT active wafer sensors. The amplitude of the output signals was in 100 mV range (Vpp). The time of flight for each wave package was picked manually by observing the signals. Wave speed for each frequency was calculated using linear regression as shown in Figure 16. For frequencies from 10kHz to up to 4MHz, the wave speed vs. frequency curves were created as shown in figure 17.
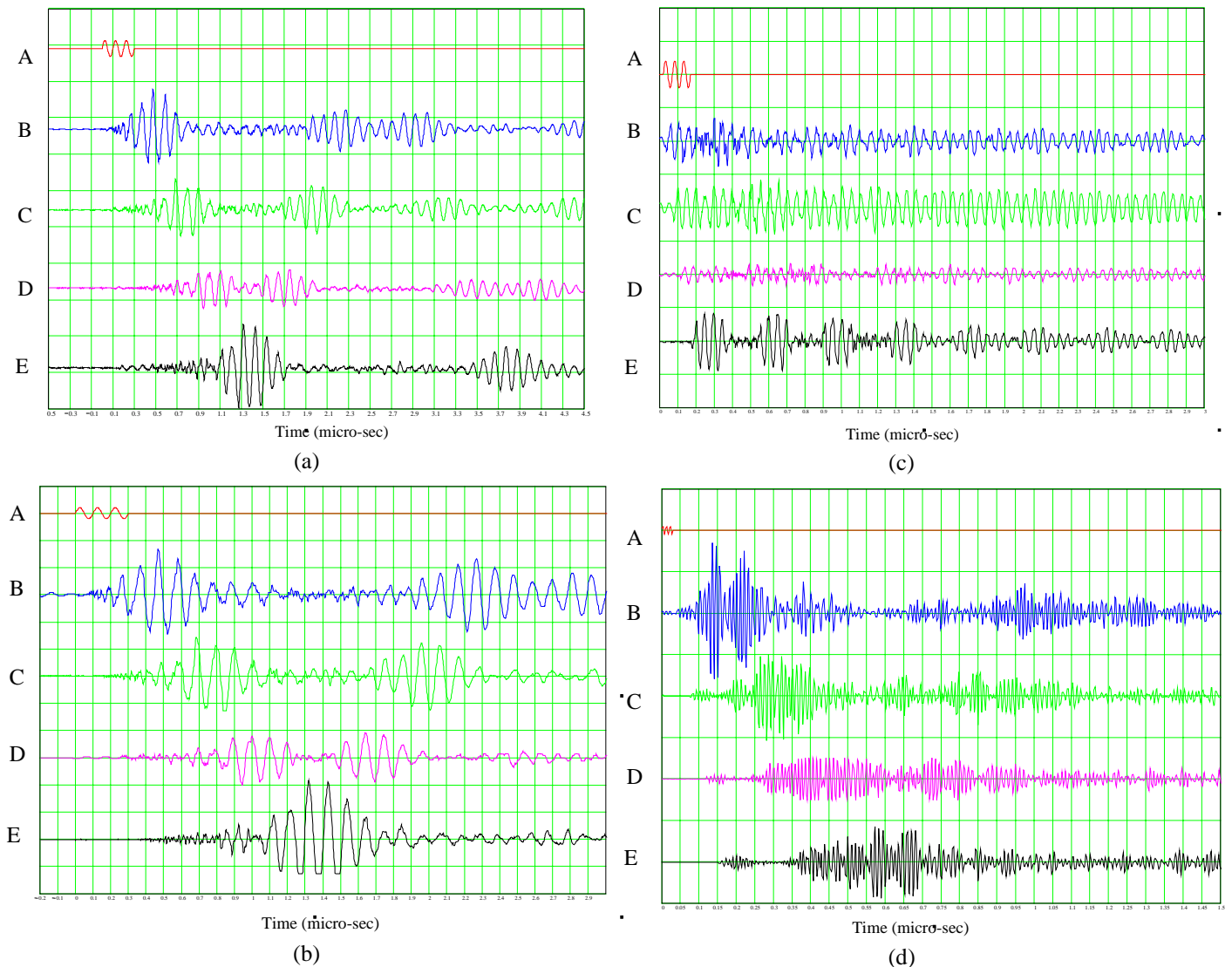

Figure 15 Experiment data from beam specimen.
(a) 10 kHz single excitation; (b) 10 kHz in-phase excitation;
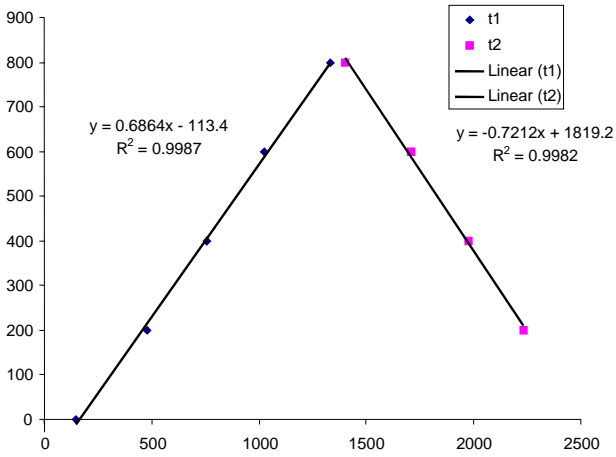(c) 10 kHz out-phase excitation; (d) 100 kHz single excitation
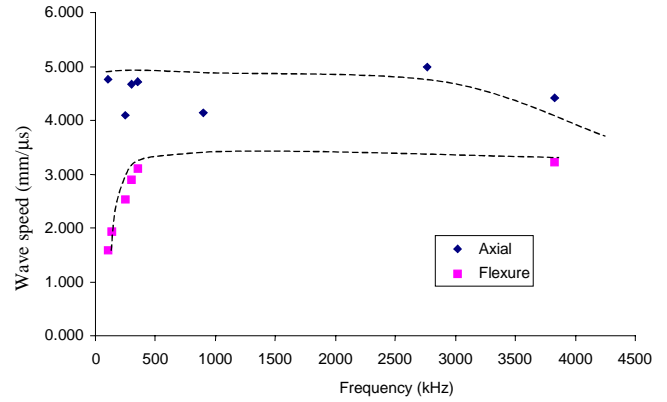
Figure 16 Wave speed analysis for 10kHz signal

Figure 17 Wave speed dispersion from experiment.

3.2.4   Experiment on realistic aging aircraft panels with simulated damages

Wave propagation experiments were conducted on realistic aircraft panel specimens with a number of PZT active sensors affixed on it at various locations. The experimental setup is shown in Figure 18. Constant-frequency 10 kHz wave bursts were sent by the transmitter active sensor, and the response was collected at seven active-sensor receptors placed at various x-y locations. The locations of the transmitter and receptors are shown in Figure 19. The transmission and reception time signals are shown in Table 3. It is apparent that the arrival time is consistent with the distance from the transmitter active sensor to the receptor active sensor. The larger the distance, the larger the time delay recorded on the Figure 20 charts. This proves that the proposed emitter-receptor damage detection strategy is viable and implementable. Also significant to mention is that the #5, #6, and #7 active-sensor receptors are not in line with the active-sensor transmitter. This verifies the assertion that the elastic waves generated by the transmitter propagate in a circular front and open the opportunity for the implementation of phase-array beam steering concepts to be explored in future experiments.
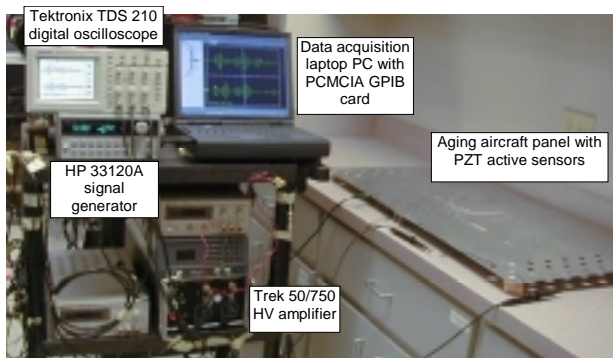

Figure 18 Experimental setup for wave propagation experiments on aging aircraft panel.
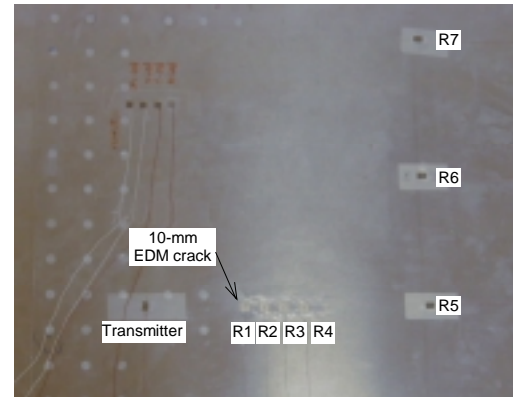

Figure 19 Installation of emitter and receptor active sensors on aging aircraft panel (sensor coordinates are given in Table 1).

Also apparent in Figure 20 is the dispersive nature of flexural waves (wave speed varies with frequency) since the wave patterns change with the distance from the transmitter. This dispersion appears because the abrupt start and stop of the 10 kHz burst used in our experiments generate side lobes in the frequency domain. These side lobes excite other frequencies besides the basic 10 kHz frequency of the burst. To reduce this effect, a fade-in/fade-out Hanning window could be used. However, this option was not available with the existing equipment. Figure 20 also displays a stray reflection that we attribute to the presence of the simulated crack. However, this crack-detection signal is buried in the other signals resulting from the signal superposition typical of low-frequency elastic waves traveling within short objects. The frequency-dependent flexural waves are reflected by the specimen boundary and become superposed over the incident waves and over the waves reflected by the simulated damage. This situation could be alleviated by using MHz range pulse excitation. At MHz frequency, the propagation speed of flexural Lamb waves reaches an asymptote, and thus the event timescale can be

expanded sufficiently to separate the incident wave from the reflection waves generated by the defect and by the specimen boundary. Thus, at MHz frequencies, the timing of pulse events has much higher resolution. However, MHz-range pulse excitation equipment, which is considerably more expensive, was not available for the experiments reported in this paper. Such equipment is currently under acquisition and will be used in future experiments.
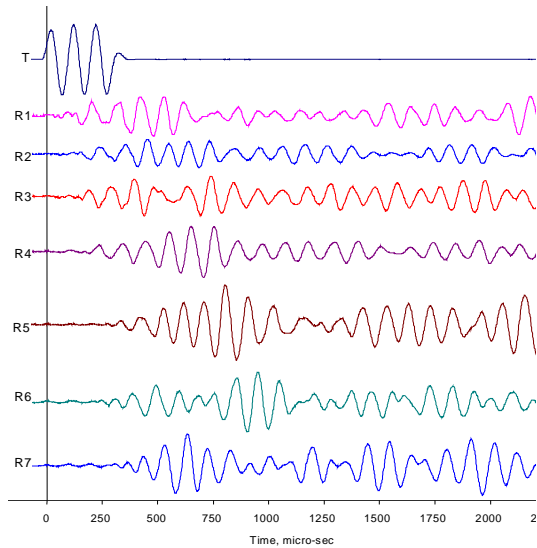

Figure 20 Transmission and reception signals for an array of PZT wafer active sensors placed at various x-y locations on the aging aircraft panel specimen (sensor coordinates are given in Table 3).
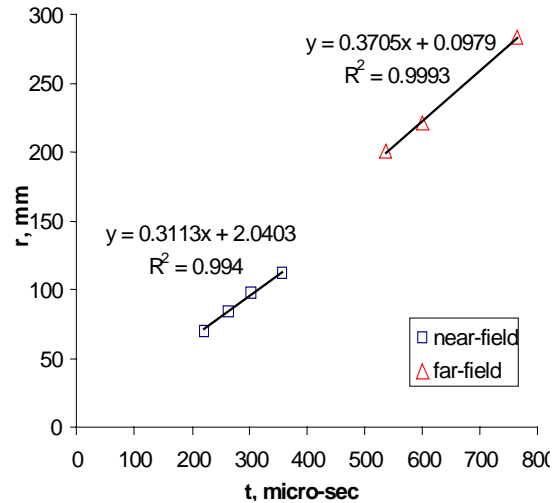

Figure 21 Wave-reception analysis: near-field and far-field time-distance correlation.

Figure 21 shows the correlation between distance and time of flight for the wave signals presented in Figure 20. Under ideal conditions, the travel distance should be directly proportional with the time of flight. The data in Figure 21 is amiable to straight-line fit with a remarkable good R^2 correlation. However, two separate groups are distinguishable, the near-field and the far-field. Nevertheless, linearity is present. The coefficient of the linear fit represents the travel speed. For the material used in these experiments (1-mm aluminum alloy sheet), the flexural wave speed at 10 kHz is 305 m/s, i.e. 0.3050 mm/μs. Figure 18 shows that the near-field speed is 0.3113 mm/μs, while the far-field speed is 0.3705 mm/μs. These results are within 2% and 21% of predictions, respectively. We conclude that, the agreement between the theory and experiment is very good for near-field, but not so good for far-field.

Table 3   Elastic wave reception data

Sensor #	x (mm)	y (mm)	r (mm)	t (μs)
1	70	0	70.0	221
2	84	0	84.0	263
3	98	0	98.0	302
4	112	0	112.0	357
5	200	0	200.0	537
6	200	96	221.8	602
7	200	201	283.6	764

The larger discrepancy observed in the far-field can be attributed to wave dispersion effects. (As discussed in the previous paragraph, wave dispersion appears due to the frequency side lobs of the square-shaped burst; this could be alleviated with a Hanning-window modulation of the burst, but the necessary equipment was not available at the time of the reported experiments). Overall, it can be concluded that the preliminary wave-propagation experiments have established that this method is a viable alternative for active-sensor damage detection. The limitations and challenges of the method have also been revealed.

4.   CONCLUSIONS

Elastic wave propagation in solid was studied theoretically and experimentally. Experiment results showed that PZT wafer active transducers could be used to generate ultrasonic wave in aluminum structures, and simultaneously collect wave propagation signals. The well-established theories and methods of ultrasonic testing can be applied to it too. This result shows that small PZT wafer transducers can take the places of traditional bulky ultrasonic transducers in some cases and can be applied to structures non-intrusively for in-situ health monitoring.

ACKNOWLEDGEMENT

REFERENCES

Blanas, P., Wenger, M. P., Shuford, R. J., and Das-Gupta, D. K., 1997. "Active Composite Materials and Damage Monitoring", *Proceedings of the International Workshop on Structural Health Monitoring*, Stanford University, CA, September 18-20, 1997, pp. 199-207.

Blanas, P., Wenger, M. P., Rigas, E. J., and Das-Gupta, D. K., 1998. "Active Composite Materials as Sensing Element for Fiber Reinforced Smart Composite Structures", *Proceedings of the SPIE North American Conference on Smart Structures and Materials*, SPIE Vol. 3329, San-Diego, CA, March 1-5, 1998.

Chahbaz A., Gauthier J., " Ultrasonic Technique for Hidden Corrosion Detection in Aircraft Wing Skin"; *Proceedings of the 3rd Joint Conference on Aging Aircraft, 1999*

Chang, F.-K., 1998, "Manufacturing and Design of Built-in Diagnostics for Composite Structures", *52nd Meeting of the Society for Machinery Failure Prevention Technology*, Virginia Beach, VA, March 30 – April 3, 1998.

Crawley, E. F. and Lazarus, K. B., 1991, "Induced Strain Actuation of Isotropic and Anisotropic Plates", *AIAA Journal*, Vol 29, No. 6, pp. 944-951.

Diaz-Valdez, S. H.; Soutis, C., 2000, "Real-Time Nondestructive Evaluation of Fiber Composite Laminates using Low-Frequency Lamb Waves", *Journal of the Acoustical Society of America* (submitted Feb. 2000)

Giurgiutiu, V., and Rogers, C. A., 1998a, "Recent Advancements in the Electro-Mechanical (E/M) Impedance Method for Structural Health Monitoring and NDE, *Proceedings of the SPIE's 5th International Symposium on Smart Structures and Materials*, 1-5 March 1998, Catamaran Resort Hotel, San Diego, CA, SPIE Vol. 3329, pp. 536-547

Giurgiutiu, V., and Rogers, C. A., 1998b, "Application of the Electro-Mechanical (E/M) Impedance Method to Machinery Failure Prevention", *Proceedings of the 52nd Meeting of the Society for Machinery Failure Prevention Technology*, March 30 – April 2, 1998, Cavalier Hotel, Virginia Beach, VA, pp. 271-280.

Graff, F., Karl, "Wave Motion in Elastic Solids"; Oxford University Press, 1975

Hall, D. L. and Flatau, A. B., 1998, "Analog feedback control for magnetostrictive transducer linearization", *Journal of Sound and Vibration*, **211**(3), pp. 481-494.

Jia, J. and Rogers, C. A., 1989, "Formulation of a Laminated Shell Theory Incorporating Embedded Distributed Actuators", ASME AD-Vol. 15, *Adaptive Structures*, B. K. Wada (Ed.), 1989.

Jiang, Zhongwei, *et al.*, "Longitudinal wave propagation Measureing Techinique fo rStructural Health Monitoring", *Proceedings of the SPIE Conference on Smart Structures and Integrated Systems,* Newport Beach, CA, March 1999

Kawiechi, Grzegorz, "Feasibility of Applying Distributed Piezotransducers to Structural Damage Detection"; *Journal of Intelligent Material Systems and Structures, Vol. 9, 1998*

Keilers, C. H., Chang, F.-K., 1995, "Identifying Delamination in Composite Beams Using Built-in Piezoelectrics: Part I - Experiments and Analysis; Part II An Identification Method", *Journal of Intelligent Material Systems and Structures*, Vol. 6, pp. 649-672, September, 1995.

Kolsky, H., "Stress Waves In Solids", Dover Publications, Inc., 1963

Lakshmanan, K. A. and Pines, D. J., 1997, "Modeling Damage in Composite Rotorcraft Flexbeams Using Wave Mechanics", *Journal of Smart Materials and Structures* (in press)

Lester, H. C., and Lefebvre, S., 1993, "Piezoelectric Actuator Models for Active Sound and Vibration Control of Cylinders", *Journal of Smart Materials and Structures*, Vol. 4, July 1993, pp. 295-306.

Liang, C., F. P. Sun, and C. A. Rogers, 1996. "Electro-mechanical Impedance Modeling of Active Material Systems," *Smart Materials and Structures*, Vol. 5, pp. 171-186.

Osmont, D.; Devillers, D.; Taillade, F. (2000) "A Piezoelectric Based Health Monitoring System for Sandwich Plates Submitted to Damaging Impacts", *European Congress of Computational Methods in Applied Sciences and Engineering ECCOMAS 2000*, Barcelona, 11-14 September 2000.

Pardo de Vera, C. and Guemes, J. A., 1997, "Embedded Self-Sensing Piezoelectrics for Damage Detection", *Proceedings of the International Workshop on Structural Health Monitoring*, Stanford University, CA, September 18-20, 1997, pp. 445-455.

Poletti, M., Linearly Swept Frequency Measurements and the Wigner-Ville Distribution, Time-Frequency Signal Analysis(ed.by Boashash, B.,),pp.424-443, Wiley Halsted Press, 1993

Quattrone, R., Berman, J., and Kamphaus, J., 1998a, "Upgrade and Monitoring of Unreinforced Masonry Structures Using Fiber Reinforced Polymers", *Proceeding of the 1998 International Composites Expo*, January 19-21, 1998, Nashville, TN, pp. 13-C/1-7.

Quinn, P., Palacios, L., Carman, G., Speyer, J., 1999, "Health Monitoring of Structures Using Directional Piezoelectrics", *1999 ASME Mechanics and Materials Conference*, June 27-30, 1999, Blacksburg, VA.

Royston, T. J, 1998, "Nonlinear Dynamics of Smart Materials Used for Structural Vibro-Acoustic Control", NSF CAREER award # 9733565, 1998-2002 (in progress).

Saravanos, D. A., Birman, V., and Hopkins, D. A., 1996, "Detection of Delamination in Composite Beams Using Piezoelectric Sensors", *Report # LEW-16308*, NASA LeRC, , OH 44135

Saravanos, D. A., Heyliger, P. R., 1995 "Coupled Layerwise Analysis of Composite Beams with Embedded Piezoelectric Sensors and Actuators", *Journal of Intelligent Material Systems and Structures*, Vol. 6, No.3, pp. 350-363, May 1995.

Tzou, H. S., and Tseng, C. I., 1990, "Distributed Piezoelectric Sensor/Actuator Design for Dynamic Measurement/Control of Distributed Parametric Systems: A Piezoelectric Finite Element Approach", *Journal of Sound and Vibration*, No. 138, pp. 17-34, 1990.